

## X-RAY EMISSION FROM THE NEARBY PSR B1133+16 AND OTHER OLD PULSARS

O. KARGALTSEV, G. G. PAVLOV, AND G. P. GARMIRE

The Pennsylvania State University, 525 Davey Lab, University Park, PA 16802, USA

*Draft version December 3, 2018*

### ABSTRACT

We detected a nearby ( $d = 360$  pc), old ( $\tau = 5$  Myr) pulsar B1133+16 with *Chandra*. The observed pulsar's flux is  $(0.8 \pm 0.2) \times 10^{-14}$  ergs cm $^{-2}$  s $^{-1}$  in the 0.5–8 keV band. Because of the small number of counts detected, the spectrum can be described by various models. A power-law fit of the spectrum gives a photon index  $\Gamma \approx 2.5$  and an isotropic luminosity of  $1.4 \times 10^{29}$  ergs s $^{-1}$  in the 0.5–8 keV band, which is about  $1.6 \times 10^{-3}$  of the spin-down power  $\dot{E}$ . The spectrum can also be fitted by a blackbody model with a temperature of  $\approx 2.8$  MK and a projected emitting area of  $\sim 500$  m $^2$ , possibly a hot polar cap. The X-ray properties of PSR B1133+16 are similar to those of other old pulsars observed in X-rays, particularly the drifting pulsar B0943+10.

*Subject headings:* pulsars: individual (PSR B1133+16) — stars: neutron — X-rays: stars

### 1. INTRODUCTION

Models of neutron star (NS) cooling (e.g., Yakovlev & Pethick 2004) predict that at an age of  $\gtrsim 1$  Myr at least passively cooling NSs become too cold to emit X-rays from the bulk of NS surface. Therefore, X-ray emission from isolated radio pulsars of such old ages is expected to consist of a magnetospheric component and, possibly, a thermal component emitted from small areas (polar caps [PCs]) heated by relativistic particles created in the pulsar's acceleration zones (e.g., Harding &Muslimov 2001, 2002; hereafter HM01 and HM02). Hence, studying the X-ray emission from old pulsars allows one to examine the properties and evolution of magnetospheric radiation, probe the particle acceleration mechanisms operating in the magnetospheres, and constrain the PC heating and emission models.

Although most of the  $\sim 1600$  currently known radio pulsars are older than 1 Myr (see Fig. 1), they are intrinsically faint X-ray sources because the luminosities of both the magnetospheric and PC components are fractions of the spin-down power  $\dot{E}$ , which decreases with pulsar's age. So far, only seven pulsars with characteristic ages  $\tau \equiv P/(2\dot{P}) > 1$  Myr have been detected in X-rays<sup>1</sup> (i.e., about 10% of X-ray detected “ordinary” pulsars), all of them at distances  $< 2$  kpc (Zavlin & Pavlov 2004 [hereafter ZP04]; Becker et al. 2004, 2005; Zhang et al. 2005; Ögelman & Tepedelenlioğlu 2005).

In principle, the magnetospheric and PC components of X-ray radiation can be distinguished by their spectra and pulse shapes (e.g., the magnetospheric radiation is expected to have a harder spectrum and show sharper pulsations). However, even the brightest of the detected old pulsars are too faint to establish the spectral shape unambiguously. For instance, the spectrum of the relatively bright PSR B0950+08 ( $d = 260$  pc,  $\tau = 17$  Myr,  $F_{0.2-10\text{ keV}} = 1.1 \times 10^{-13}$  ergs s $^{-1}$  cm $^{-2}$ ), observed re-

cently with *XMM-Newton*, can be fitted with either a single power-law (PL) model with photon index  $\Gamma \approx 1.75$  or a combination of a PL model ( $\Gamma \approx 1.35$ ) and a thermal (hydrogen atmosphere) model, with PC temperature  $T_{\text{pc}} \sim 1$  MK and radius  $R_{\text{pc}} \sim 250$  m (the two-component interpretation is supported by the energy-dependent pulse shape; ZP04). Therefore, it is important to observe a larger sample of old pulsars and study their properties via comparative analysis.

In this *Letter*, we report on first X-ray detection of one of the nearest pulsars, PSR B1133+16 (= J1136+1551; see Table 1 for the radio pulsar parameters). This old pulsar ( $\tau = 5$  Myr) has the largest proper motion, 375 mas yr $^{-1}$ , among the known radio pulsars, which corresponds to the transverse velocity  $V_{\perp} \simeq 630$  km s $^{-1}$  at the distance of 360 pc inferred from the radio parallax measurement (Brisken et al. 2002). The pulsar shows a double-peaked radio pulse, and it is known to spend  $\simeq 15\%$  of the time in a “null state” where it does not emit radio pulses (Biggs 1992). From radio polarization observations, Lyne & Manchester (1988) infer the angle  $\alpha = 51.3^\circ$  between the magnetic and rotation axes, and the angle  $\beta = 3.7^\circ$  of the closest approach of the magnetic axis to the line of sight. Although the pulsar's spin-down power,  $\dot{E} = 8.8 \times 10^{31}$  ergs s $^{-1}$ , is smaller than those of the other pulsars detected in X-rays, its “spin-down flux”,  $\dot{E}/(4\pi d^2) = 5.8 \times 10^{-12}$  erg s $^{-1}$ , is large enough to warrant an exploratory X-ray observation with *Chandra* or *XMM-Newton*. We describe a *Chandra* observation of PSR B1133+16 and its analysis in §2 and §3 and compare the properties of this pulsar with those of other old pulsars in §4.

### 2. OBSERVATIONS

PSR B1133+16 (hereafter B1133) was observed with the Advanced CCD Imaging Spectrometer (ACIS) on 2005 February 23 (start time 53,424.79 MJD). The useful scientific exposure time was 17,911 s. The observation was carried out in Very Faint mode, and the pulsar was imaged at the aim point on ACIS-S3 chip. The detector was operated in full frame mode which provides time resolution of 3.2 s. The data were reduced using the *Chandra* Interactive Analysis of Observations (CIAO)

Electronic address: green@astro.psu.edu, pavlov@astro.psu.edu

<sup>1</sup> The oldest known pulsars are the recycled millisecond pulsars (MSPs) with ages 0.1–10 Gyr. Since they are spun-up by accretion in binaries, their properties may differ from those of the “ordinary” old isolated pulsars; therefore, we do not consider MSPs in this paper.

TABLE 1  
OBSERVED AND DERIVED PARAMETERS FOR PSR B1133+16

Parameter	Value
R.A. (J2000).....	11 <sup>h</sup> 36 <sup>m</sup> 03 <sup>s</sup> .1829(10)
Dec. (J2000).....	+15°51'09".726(15)
Epoch of position (MJD).....	51,544.0
Proper motion, R.A./Dec. (mas yr <sup>-1</sup> )..	-73.95(38)/368.05(28)
Spin period, $P$ (s).....	1.1879
Dispersion Measure, DM (cm <sup>-3</sup> pc).....	4.86
Distance from parallax, $d$ (pc).....	357(19)
Surface magnetic field, $B_s$ (10 <sup>12</sup> G).....	2.13
Spin-down power, $\dot{E}$ (10 <sup>31</sup> erg s <sup>-1</sup> ).....	8.8
Age, $\tau = P/(2\dot{P})$ , (Myr).....	5.04

NOTE. — Based on the data from the ATNF radio pulsar catalog (Manchester et al. 2005). The position, proper motion, and distance are from Brisken et al. (2002). The numbers in parentheses represent uncertainties in the last significant digits.

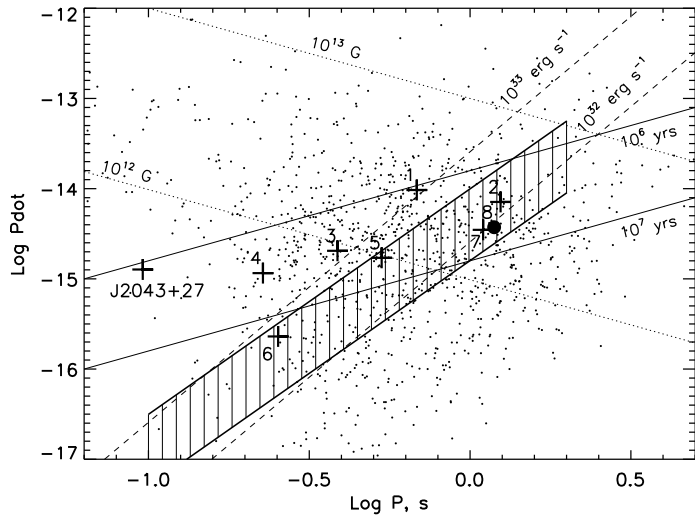


FIG. 1.—  $P$ - $\dot{P}$  diagram for  $\approx 1400$  radio pulsars (dots) from the ATNF catalog (Manchester et al. 2005). Lines of constant pulsar age, magnetic field, and  $\dot{E}$  are shown. Eight pulsars with  $\tau > 1$  Myr that have been previously observed in X-rays are marked by crosses, and PSR B1133+16 is marked by the filled circle. The numbers, 1 through 8, near the marked pulsars correspond to those in Fig. 5. The hatched area represents plausible locations of the death line for the curvature radiation induced cascade (from eqn. [52] of HM02, for pair production efficiencies in the 0.2–0.5 range.)

software (ver. 3.2.1; CALDB ver. 3.0.3).

### 3. X-RAY IMAGE AND SPECTRUM

Figure 2 shows the ACIS-S3 image of the B1133 field. The X-ray source is clearly seen at R.A.= 11<sup>h</sup>36<sup>m</sup>03<sup>s</sup>.169, Dec.= +15°51'11".87 (centroid uncertainty is 0''.2). This position is within 0''.1 of the radio position of B1133 derived from its proper motion at the epoch of the *Chandra* observation. Therefore, we conclude with confidence that we detected the pulsar's X-ray counterpart. The distribution of source counts in the image is consistent with that of a point source.

We extracted the pulsar's spectrum from a circular aperture with the radius of 2.5 ACIS pixels ( $= 1''.23$ ;  $\approx 90\%$  encircled energy radius) using the CIAO *psextract*

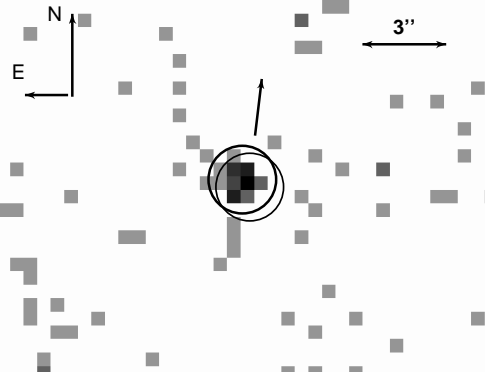


FIG. 2.— ACIS-S3 image of PSR B1133+16. The two circles are centered at the centroid of the source count distribution and the pulsar's position predicted from its proper motion. The arrow shows the direction of the proper motion; its length corresponds to the pulsar's displacement during 6 years.

task. The background was extracted from  $5'' < r < 22''$  annulus centered on the source. The total number of counts within the source aperture is 33, of which 99.7% are expected to come from the source. The observed source flux is  $(0.8 \pm 0.2) \times 10^{-14}$  ergs cm<sup>-2</sup> s<sup>-1</sup> in the 0.5–8 keV band. We group the counts into 7 spectral bins (4–5 counts per bin; see Fig. 3) and fit the spectrum with absorbed PL and blackbody (BB) models. Because of the small number of counts, we have to freeze the hydrogen column density,  $n_H$ . We adopt  $n_H = 1.5 \times 10^{20}$  cm<sup>-2</sup> estimated from the dispersion measure, 4.86 cm<sup>-3</sup> pc, assuming a 10% degree of ionization of the ISM. (Varying  $n_H$  in the plausible range of  $1-2 \times 10^{20}$  cm<sup>-2</sup> does not change the fits substantially.) Since each of the spectral bins has only a few counts, we fit the spectrum using the maximum likelihood method implemented in XSPEC (v. 11.3) with the C-statistic (Cash 1979). The fitting parameters for the PL and BB models are given in Table 2 while the fits and the confidence contours are shown in Figures 3 and 4.

The PL fit gives a photon index  $\Gamma = 2.2-2.9$  and an isotropic luminosity  $L_{0.5-8 \text{ keV}} = 4\pi d^2 F_{0.5-8 \text{ keV}}^{\text{unabs}} \approx 1.4 \pm 0.3 \times 10^{29}$  ergs s<sup>-1</sup>, for  $d = 357$  pc. The temperature and the projected area of the emitting region obtained from the BB fit are strongly correlated (see Fig. 4), which results in large uncertainty of these parameters. However, the projected area,  $\sim 500$  m<sup>2</sup>, is much smaller than that of a NS,  $\sim 3 \times 10^{10}$  m<sup>2</sup>, which suggests that the radiation could be emitted from hot polar caps, with an effective radius  $R \sim 13(\cos \theta)^{-1/2}$  m and a bolometric luminosity  $L_{\text{bol}} = \sigma T^4 A(\cos \theta)^{-1} = 3.2_{-0.6}^{+0.5} \times 10^{28}(\cos \theta)^{-1}$  ergs s<sup>-1</sup>, where  $\langle \cos \theta \rangle$  is a time-averaged cosine of the angle between the line of sight and the magnetic axis ( $\approx 0.47$  for the axis orientations suggested by Lyne & Manchester 1988).

### 4. DISCUSSION

The scarce statistics of the short observation of B1133 does not allow one to differentiate between the alternative spectral models. Below we explore various possibilities by invoking independent arguments such as comparison with the properties of other old pulsars observed in X-rays.

For the PL model, the photon index  $\Gamma \approx 2.5$  of the

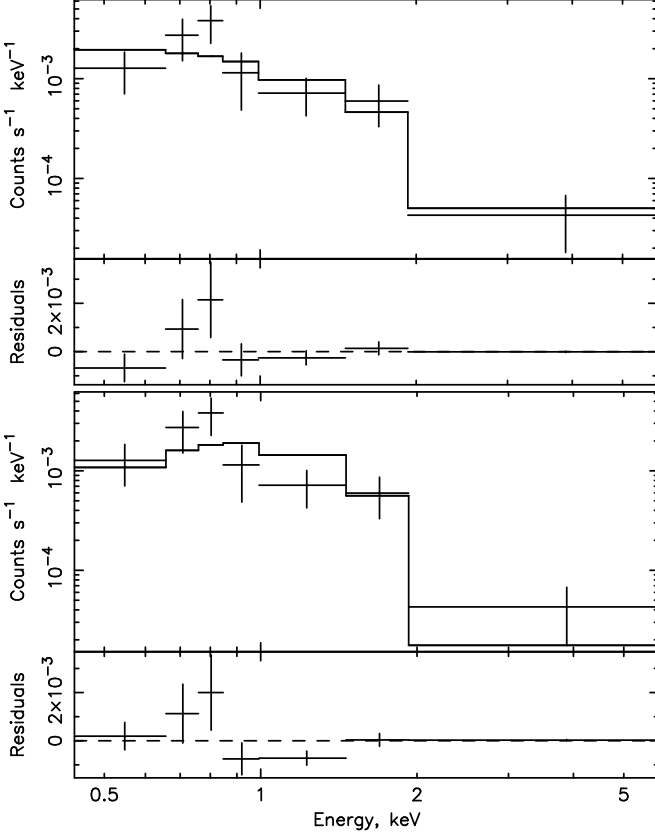


FIG. 3.— B1133 spectrum fitted with the PL (top) and BB (bottom) models. The contributions of the energy bins into the best-fit C-statistic are shown, multiplied by  $-1$  when the number of data counts is smaller than the number of model counts.

TABLE 2  
FITTING PARAMETERS FOR THE PL AND BB MODELS

Model	Norm.	$\Gamma$ or $kT$	$C/\text{dof}$	$Q$	$L_{29}$
PL	$2.66^{+0.43}_{-0.41}$	$2.51^{+0.36}_{-0.33}$	6.20/5	43%	$1.4 \pm 0.3$
BB	$0.50^{+0.30}_{-0.22}$	$0.28^{+0.04}_{-0.03}$	10.4/5	79%	$0.32^{+0.05}_{-0.06}$

NOTE. — The hydrogen column density was fixed at  $n_{\text{H}} = 1.5 \times 10^{20} \text{ cm}^{-2}$  for both the PL and BB fits. Normalization in second column is the spectral flux in  $10^{-6} \text{ photons cm}^{-2} \text{ s}^{-1} \text{ keV}^{-1}$  at 1 keV for the PL fit, and the projected area in  $10^7 \text{ cm}^2$  for the BB fit. Third column gives the photon index for the PL fit and the temperature in keV for the BB fit. Fourth column gives the best-fit value of C-statistic and the number of degrees of freedom. The parameter  $Q$  in fifth column is the percentage of 10,000 Monte Carlo simulations, drawn from the best-fit model, which give a C-statistic value lower than the best-fit value. The last column gives the luminosities in units of  $10^{29} \text{ ergs s}^{-1}$ , for  $d = 357 \text{ pc}$  ( $L_{0.5-8 \text{ keV}}$  for the PL fit,  $L_{\text{bol}}(\cos \theta)$  for the BB fit, see text).

B1133 spectrum is somewhat larger than  $\Gamma \simeq 1-2$  observed for young and middle-aged pulsars (e.g., Gotthelf 2003). Interestingly, PL fits of some other old pulsars (e.g., B0943+10, B0628–28) also show very soft spectra, with  $\Gamma \approx 2-3$  (ZP04; Zhang et al. 2005; Ögelman, & Tepedelenlioğlu 2005), suggesting that pulsar spectra might soften with increasing age or decreasing spin-down power. However, the example of PSR B0950+08, the oldest in the sample, demonstrates that the softness of the one-component PL fit may be caused by the presence of a thermal (PC) component, which mostly con-

tributes at lower energies: a single PL fit gives  $\Gamma \approx 1.8$  for PSR B0950+08, while the slope of the PL component in the two-component fit is  $\approx 1.3$ , similar to younger pulsars (ZP04).

The extrapolation of the X-ray PL fit into the optical range predicts easily detectable optical magnitudes (e.g.,  $V \sim 20-24$  mag). A more realistic prediction,  $V \sim 29-30$  mag, can be obtained from the empirical relation between the optical and X-ray fluxes of spin-powered pulsars (ZP04).

The luminosity found from the PL fit allows one to estimate the “X-ray efficiency” for B1133:  $\eta \equiv L_X/\dot{E} = 1.6(-0.4, +0.3) \times 10^{-3}$  in the 0.5–8 keV band ( $\eta = 1.0 \pm 0.3 \times 10^{-3}$  and  $0.6 \pm 0.2 \times 10^{-3}$  in the 1–10 and 2–10 keV bands, respectively). The inferred efficiency is larger than for most young and middle-aged pulsars (e.g., Possenti et al. 2002), but it is within the range of efficiencies found for other old pulsars (ZP04). We plot in Figure 5 the 1–10 keV luminosities of eight old pulsars, as inferred

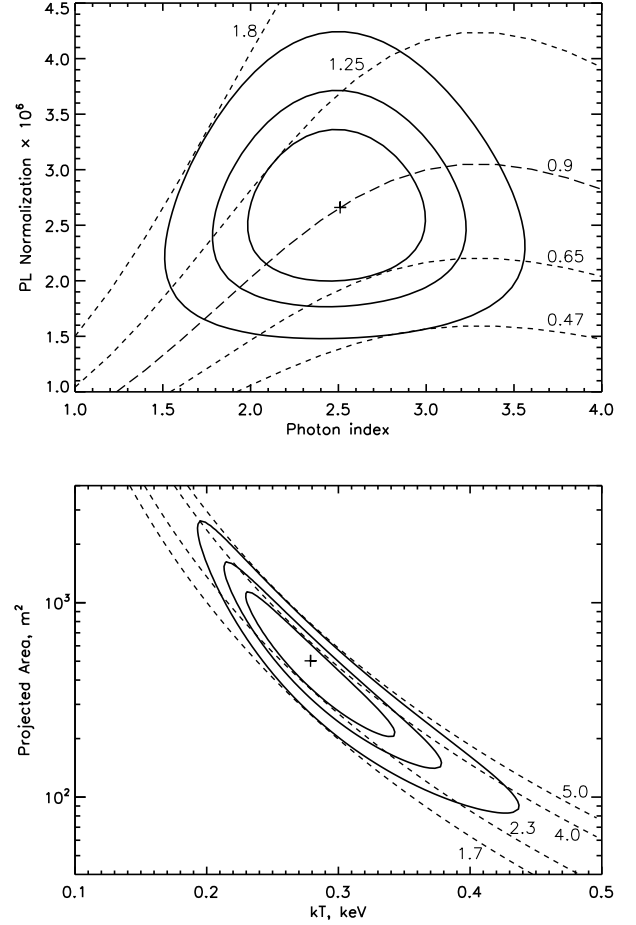


FIG. 4.— Confidence contours (68%, 90%, and 99%, computed for two interesting parameters) for the PL (top) and BB (bottom) model fits to the ACIS spectrum of PSR B1133+16. The PL normalization is in units of  $10^{-6} \text{ photons cm}^{-2} \text{ s}^{-1} \text{ keV}^{-1}$  at 1 keV. The BB normalization (vertical axis) is the projected emitting area in units of  $\text{m}^2$ , for  $d = 357 \text{ pc}$ . The lines of constant unabsorbed flux (PL model; in units of  $10^{-14} \text{ erg cm}^{-2} \text{ s}^{-1}$ ) and constant bolometric luminosity (BB model; for  $\langle \cos \theta \rangle = 1$ , in units of  $10^{28} \text{ erg s}^{-1}$ ) are plotted as dashed lines, for fixed  $n_{\text{H}} = 1.5 \times 10^{20} \text{ cm}^{-2}$ .

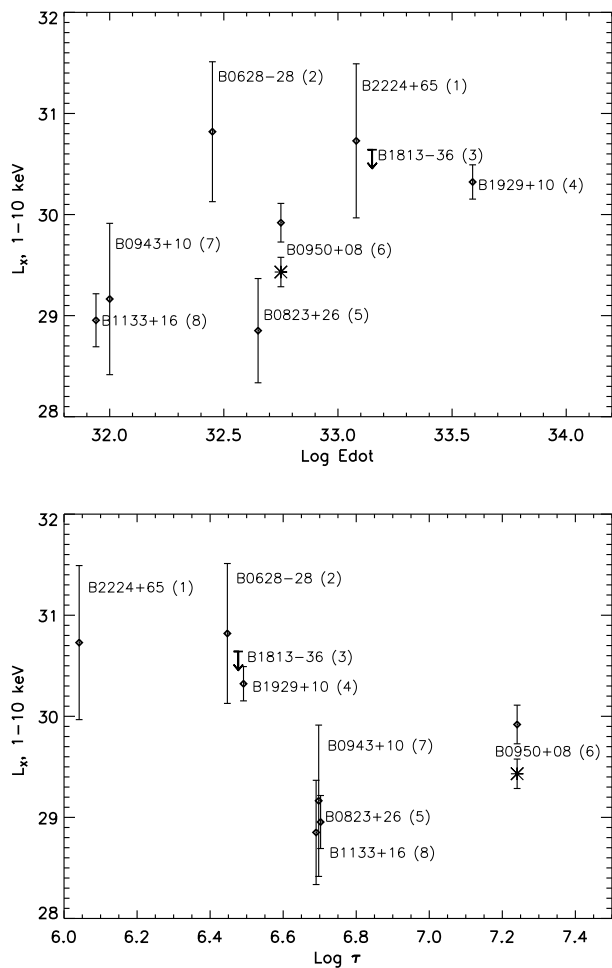


FIG. 5.— The X-ray luminosities (1–10 keV band) of eight old pulsars versus spin-down power (top) and characteristic age (bottom). The numbers in parentheses correspond to the pulsars marked in Fig. 1. For PSR B0950+08, the diamond and the asterisk show the luminosities of the nonthermal and thermal components, respectively (as determined from the PL+NSA fit by ZP04). For the other pulsars, the luminosities were obtained from PL fits found in the literature (ZP04; Ögelman, H., & Tepeledenlioglu 2005; Becker et al. 2004, 2005; Zhang et al. 2005) or remeasured from the *Chandra* data. PSR B1813–36 was not detected in a 30 ks *Chandra* exposure, hence only the upper limit is plotted.

from the PL fits, versus spin-down power and characteristic age<sup>2</sup>. For the pulsars whose parallaxes have not been measured, we ascribe a factor of 2 uncertainty to the distances estimated from the pulsar's dispersion measure. Although the luminosity shows some correlation with  $\dot{E}$ , the scatter is quite substantial (for instance, the luminosities of B0628–28 and B0823+26 differ by about 2 orders of magnitude despite the close values of  $\dot{E}$ ). Such a scatter can possibly be attributed to different orientations of the pulsar beams with respect to the observer. Overall, the apparent X-ray efficiencies of the observed

<sup>2</sup> We exclude PSR J2043+2740 from this sample because its predominantly thermal X-ray spectrum resembles those of middle-aged pulsars rather than of old ones (ZP04). Possibly, its characteristic age,  $\tau = 1.2$  Myr, is larger than its actual age. Notice that its position on the  $P$ – $\dot{P}$  diagram is also quite different from those of the other pulsars in the sample (see Fig. 1).

old pulsars are somewhat higher than those of younger pulsars, but this can be caused by the selection effect (the sample is biased in favor of brighter objects). The correlation of the luminosity with the characteristic age is even less pronounced; for instance, the luminosity of the oldest PSR B0950+08 ( $\tau = 17$  Myr) is a factor of 10 higher than those of PSRs B1133+16, B0943+10, and B0823+26 ( $\tau \approx 5$  Myr). We should remember, however, that the characteristic age can be substantially different from the true age, so the dependence  $L_X(\tau)$  may not accurately characterize the pulsar evolution.

The best-fit temperature,  $\approx 2.8$  MK, obtained from the BB fit to the spectrum of B1133, is close to  $\approx 3.1$  MK and  $\approx 1.8$  MK obtained from the BB fit for PSR B0943+10 and BB+PL fit for PSR B0950+08, respectively. Although the effective radius of the emitting region,  $R_{\text{BB}} \sim 19$  m, is highly uncertain because of poor statistics, it is certainly smaller than the conventional PC radius assuming a dipole magnetic field,  $R_{\text{pc}} = (2\pi R^3/cP)^{1/2} \simeq 130$  m. A similar discrepancy is also seen in the above-mentioned fits to the spectra of B0943+10 ( $R_{\text{BB}} \sim 20$  m,  $R_{\text{pc}} \simeq 140$  m) and B0950+08 ( $R_{\text{BB}} \sim 50$  m,  $R_{\text{pc}} \simeq 290$  m). Zhang et al. (2005) suggest that the small X-ray emitting area can be explained assuming that only a small fraction of the PC area is heated by the inflowing relativistic particles created in “spark discharges” above the PC (Ruderman & Sutherland 1975). An independent support of this interpretation is provided by the subpulse drifting observed in B0943+10. No subpulse drifting has been reported for B1133+16, but this may be the result of a different orientation of the pulsar beam. The discrepancy can also be caused by a PC thermal spectrum being different from the blackbody. For instance, fits with the magnetic hydrogen atmosphere (NSA) models (Pavlov et al. 1995) usually give a factor of 2 lower temperatures and a factor of 5–10 larger radii, with about the same observed luminosity. ZP04 explored this possibility for PSR B0950+08 and obtained a temperature of  $\approx 1.1$  MK and an emitting radius of 250 m, close to the  $R_{\text{pc}} = 290$  m. We do not attempt to fit the spectrum of B1133 with the NSA models because too few counts were detected and, with the time resolution of 3.2 s, we cannot extract the light curves of the 1.19 s pulsations needed for an accurate analysis of the highly anisotropic atmosphere radiation.

As one can see from Table 2 and Figure 3, the quality of the BB fit is worse than that of the PL fit because of an excess of observed counts at  $E > 1.5$  keV. This indicates that the spectrum might have both thermal and nonthermal (PL) components, similar to those seen in many younger pulsars and, likely, in the old B0950+08 (Pavlov et al. 2002; ZP04). It is very likely that the radiation of the other old pulsars, from which too few counts have been detected to firmly establish the origin of their X-ray emission, also consists of both thermal and nonthermal components. If this is the case, the luminosities inferred from the BB fits should be considered as upper limits. The current upper limits on bolometric BB luminosities are close to the 1–10 keV PL luminosities shown in Figure 5.

If the X-ray radiation from B1133 is dominated by the thermal emission from PCs, then its PC efficiency is  $\eta_{\text{pc}} \equiv L_{\text{bol}}/\dot{E} = 3.6_{-0.7}^{+0.6} \times 10^{-4} (\cos \theta)^{-1}$  ( $\sim 8 \times 10^{-4}$

for  $\langle \cos \theta \rangle = 0.47$ ). This efficiency is two orders of magnitude lower than those predicted by HM01 models for the curvature radiation (CR) induced pair cascade (Fig. 7 of HM01), which might indicate that the CR cascade does not operate in B1133. Indeed, this pulsar is very close to the “CR death line” in the  $P$ - $\dot{P}$  diagram (see Fig. 1), perhaps even below it, depending on exact value of pair production efficiency (see HM01 for details). Note, however, that the PC luminosities for the CR cascade derived by Arons (1981) under somewhat different assumptions underestimate the observed  $\eta_{\text{pc}}$  by a factor of 100. The PC efficiencies expected from the less efficient inverse Compton scattering (ICS) cascade, which may play some role below the CR death line (see HM02), are also 1–2 orders of magnitude lower than our observational estimate. Therefore, if B1133 lies below the CR death line, then the observed emission is most likely produced in the magnetosphere.

To summarize, the X-ray spectrum of B1133 can be described by either a nonthermal PL model or a thermal BB model, or a combination of those. The X-ray pa-

rameters of B1133 are particularly close to those of PSR B0943+10, which is almost a twin of B1133+16 in terms of  $P$  and  $\dot{P}$  also. The nonthermal X-ray efficiencies of B1133 and other old pulsars generally exceed those of younger pulsars, but it is currently unclear whether this is a genuine property or it is caused by selection effects. PL fits of old pulsars show, on average, steeper spectra, but this may be caused by the presence of a thermal component. If the predictions of the current pair cascade models are correct, then either the CR cascade is still operating in B1133 and X-rays are emitted from the heated NS surface, or the bulk of X-ray emission is produced in the pulsar’s magnetosphere. Since B1133 is a typical representative of the majority of radio pulsars, it would be important to better constrain its X-ray properties in a deeper observation.

This work was partially supported by NASA grants NAG5-10865 and NAS8-01128 and *Chandra* award SV4-74018.

#### REFERENCES

Arons, J. 1981, *ApJ*, 248, 1099  
 Becker, W., Weisskopf, M. C., Tennant, A. F., Jessner, A., Dyks, J., Harding, A. K., Zhang, S. N. 2004, *ApJ*, 615, 908  
 Becker, W., Kramer, M. C., Jessner, A., et al. 2005, submitted to *ApJ*, astro-ph/0506545  
 Biggs, J. D. 1992, *ApJ*, 394, 574  
 Brisken, W. F., Benson, J. M., Gross, W. M., & Thorsett, S. E. 2002, *ApJ*, 571, 906  
 Harding, A. K., & Muslimov, A. G. 2001, *ApJ*, 556, 987 (HM01)  
 Harding, A. K., & Muslimov, A. G. 2002, *ApJ*, 568, 862 (HM02)  
 Cash, W. 1979, *ApJ*, 228, 939  
 Gotthelf, E. V. 2003, *ApJ*, 591, 361  
 Lyne, A. G., & Manchester, R. N. 1988, *MNRAS*, 234, 477  
 Manchester, R. N., et al. 2005, *AJ*, 129, 1993  
 Ögelman, H., & Tepeledenlioglu, E. 2005, *ApJ Lett.*, in press (astro-ph/0505461)  
 Pavlov, G. G., Shibanov, Yu. A., Zavlin, V. E., & Meyer, R. 1995, in *The Lives of the Neutron Stars*, ed. M. A. Alpar, Ü. Kizilöglü & J. van Paradijs (Dordrecht: Kluwer), 71  
 Pavlov, G. G., Zavlin, V. E., & Sanwal, D. 2002, in *Proc. 270 Heraeus Seminar on Neutron Stars, Pulsars, and Supernova Remnants*, ed. W. Becker, H. Lesch, & J. Trümper (MPE Rep. 278; Garching: MPE), 283  
 Possenti, A., Cerutti, R., Colpi, M., & Mereghetti, S. 2002, *A&A*, 387, 993  
 Ruderman, M., & Sutherland, P. G. 1975, *ApJ*, 196, 51  
 Yakovlev, D.G., & Pethick, C. J. 2004, *ARA&A*, 42, 169  
 Zavlin, V. E., & Pavlov, G. G. 2004, *ApJ*, 616, 452 (ZP04)  
 Zhang, B., Sanwal, D., & Pavlov, G. G. 2005, *ApJ*, 624, L109